

A native to amyloidogenic transition regulated by a backbone trigger

Catherine M Eakin^{1,2}, Andrea J Berman¹ & Andrew D Miranker¹

Many polypeptides can self-associate into linear, aggregated assemblies termed amyloid fibers. High-resolution structural insights into the mechanism of fibrillogenesis are elusive owing to the transient and mixed oligomeric nature of assembly intermediates. Here, we report the conformational changes that initiate fiber formation by β -2-microglobulin (β 2m) in dialysis-related amyloidosis. Access of β 2m to amyloidogenic conformations is catalyzed by selective binding of divalent cations. The chemical basis of this process was determined to be backbone isomerization of a conserved proline. On the basis of this finding, we designed a β 2m variant that closely adopts this intermediate state. The variant has kinetic, thermodynamic and catalytic properties consistent with its being a fibrillogenic intermediate of wild-type β 2m. Furthermore, it is stable and folded, enabling us to unambiguously determine the initiating conformational changes for amyloid assembly at atomic resolution.

Formation of amyloid fibers results from conformational changes to a normally soluble protein that permit self-assembly into an aggregated filamentous state^{1,2}. Amyloid structures are long lived and unusually resistant to dissociation and enzymatic degradation. These properties have been capitalized upon for diverse functions in organisms ranging from *Escherichia coli* to humans^{3–5}. Most proteins, however, are under selective pressure to avoid this phenomenon^{6,7}, particularly as the intermediates to fiber formation are cytotoxic⁸. As a result, fiber formation is most prevalent in diseases associated with advancing age, such as Alzheimer disease, and diseases associated with medical therapy, such as dialysis-related amyloidosis (DRA).

Amyloid formation across diverse systems follows a characteristic kinetic profile to yield fibers with very similar molecular organizations. Assembly kinetics are nucleation dependent, characterized by a lag phase that precedes rapid and apparently cooperative association. The lag phase can typically be bypassed by the addition of exogenous fibers to a reaction. Regardless of the starting conformational state of the precursor, all amyloid fibers share a common core structure⁹. This structure is cross- β , in which an assembly of β strands is arranged into sheets with the strands running perpendicular to the fiber's long axis and backbone hydrogen bonding running parallel. These commonalities strongly suggest the presence of recurring motifs in the mechanisms of assembly.

The fibrous component of amyloid deposits in DRA is β 2m. β 2m is the \sim 12-kDa polypeptide subunit necessary for the cell-surface expression of the class I-like complexes, including the major histocompatibility complex (MHC)^{10,11}. β 2m has a seven-stranded β -sandwich fold typical of the immunoglobulin superfamily. Three β -strands (C, F and G) form one side of the sandwich and four (A, B,

E and D) form the other. An internal disulfide bond tethers strands B and F together in the folded protein (Fig. 1a). As part of cell turnover, β 2m is released from the MHC and circulates in the sera at \sim 0.1 μ M, where it is then catabolized by the kidney. In renal disease patients, β 2m concentrations increase up to ten-fold and β 2m deposits as amyloid in the joint spaces¹². Although an increase in concentration may contribute to amyloid assembly, it is not sufficient for it: β 2m concentrations can be elevated in diseases not associated with amyloidosis^{13–15}, and purified β 2m is folded and soluble even at millimolar concentrations^{16,17}. *In vitro*, β 2m has been converted into fibers by acidification¹⁸ and through the use of truncated fragments^{19,20}. However, under native solution conditions comparable with human serum (150 mM salt, pH 7.4, 37 °C)²¹, wild-type (WT) β 2m fibers have been shown to form only with the addition of stoichiometric copper¹⁵. As Cu^{2+} concentrations in hemodialysate are permitted to be as high as 1.6 μ M²², reducing the allowed Cu^{2+} concentration may decrease the incidence or severity of this disease.

In this study, we set out to establish the chemical and structural basis of the changes in human β 2m required for oligomeric assembly. The first step²³ in β 2m amyloid formation is conversion of the native state (M) to an alternative native-like conformation, termed M* (Fig. 1b). Cu^{2+} -catalyzed formation of M* occurs on the timescale of 1 h. This is followed by immediate assembly into di-, tetra- and hexameric states that are stabilized by Cu^{2+} and therefore reversible upon metal chelation. These states are collectively termed oligomers in this work. The requirement for Cu^{2+} is, however, only transient, as oligomers transition to fiber on the timescale of 1 week²³ (at 2:1 Cu^{2+} / β 2m; Supplementary Fig. 1 online), whereupon the sensitivity to

¹Department of Molecular Biophysics and Biochemistry, Yale University, 260 Whitney Avenue, New Haven, Connecticut 06520-8114, USA. ²Present address: Department of Biochemistry and Biomolecular Structure Center, University of Washington, K464 Health Science Building, Box 357350, Seattle, Washington, 98195-7742, USA. Correspondence should be addressed to A.D.M. (andrew.miranker@yale.edu).

Received 28 November 2005; accepted 18 January 2006; published online 19 February 2006; doi:10.3892/nsmb1068

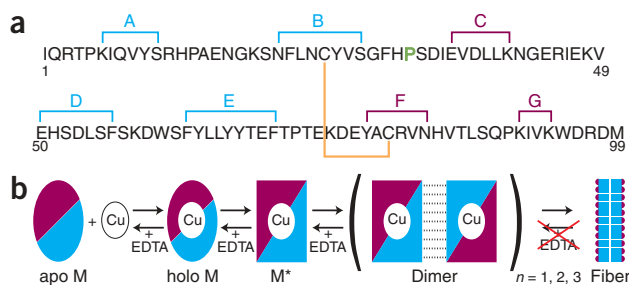


Figure 1 Mechanism and structural basis of Cu^{2+} binding and amyloid assembly. **(a)** Primary sequence of human $\beta 2\text{m}$ showing strand nomenclature. Two sets of β -strands with connectivity ABED and CFG form a β -sandwich. The internal disulfide bond is shown in orange. **(b)** Simplified schematic of steps for Cu^{2+} -associated $\beta 2\text{m}$ amyloid assembly²³.

chelate is lost (**Fig. 1b**). Here, we have determined the chemical basis of, and characterized at atomic resolution, the structural changes for the conversion of M to M^* , the initial step of $\beta 2\text{m}$ amyloidosis.

RESULTS

M^* is kinetically isolated

Formation of the M^* state of $\beta 2\text{m}$ is a structurally specific consequence of Cu^{2+} binding. This was apparent from the kinetics of oligomeric assembly monitored using the dye thioflavin T (ThT)²⁴ (**Fig. 2a**). Incubation of 100 μM $\beta 2\text{m}$ with 200 μM Cu^{2+} resulted in an exponential profile with a time constant $\tau = 630 \pm 20$ s. Once formed, the oligomers are stable for hours, enabling discrete peaks to be observed by size-exclusion chromatography (data not shown) and by sedimentation-velocity analytical ultracentrifugation (SV) (**Fig. 2b**). Remarkably, although $\beta 2\text{m}$ binds nickel¹⁷, oligomerization was wholly absent in its presence (**Fig. 2b**). Oligomers were not detected kinetically (**Fig. 2a**), by SV (**Fig. 2b**) or by size-exclusion chromatography (data not shown) for 100 μM protein incubated with 1,000 μM Ni^{2+} (data not shown) or 300 μM Ni^{2+} . The intrinsic affinity of imidazole in aqueous solutions is about ten-fold greater for Cu^{2+} than for Ni^{2+} . Therefore, higher concentrations of Ni^{2+} relative to Cu^{2+} were used in this work to ensure that observations were not attributable to differences in Ni^{2+} and Cu^{2+} affinities. This was further confirmed in a related control, where we observed that Ni^{2+} can compete with Cu^{2+} , resulting in the loss of oligomerization activity (**Supplementary Fig. 2** online).

Discrimination between metals is mirrored in the apparent free energy of unfolding (ΔG_U). $\beta 2\text{m}$ is unusual in that it becomes destabilized in the presence of a large excess of its ligand²¹. However, whereas 90 μM Cu^{2+} destabilizes 2.5 μM $\beta 2\text{m}$ by $\Delta\Delta G = 21$ kJ mol^{-1} , the ΔG_U in the presence of 2,000 μM Ni^{2+} is within error of apo $\beta 2\text{m}$ (**Fig. 3**). The phenomena of destabilization upon ligand binding and oligomerization of native-like states are compatible with a three-state energy diagram (**Fig. 4a**). Destabilization requires that the unfolded state (U) bind Cu^{2+} with greater affinity than the folded state, M. This occurs in the presence of excess cations, as three additional imidazoles coordinate transition metal in the unfolded state, whereas only one coordinates in the native state¹⁷. The dependence of oligomerization on Cu^{2+} requires that apo M^* have a higher energy than holo M^* . As holo M^* is readily formed from holo M, the apparent ΔG_U of holo $\beta 2\text{m}$ and apo $\beta 2\text{m}$ reflects the $\text{U} \leftrightarrow \text{M}^*$ and $\text{U} \leftrightarrow \text{M}$ equilibria, respectively. Ni^{2+} is chemically similar to Cu^{2+} ; therefore, it can also bind conformations on this reaction coordinate. Nevertheless, even at concentrations elevated compared to Cu^{2+} , oligomerization is never observed

in the presence of Ni^{2+} . This suggests that the bases of cation discrimination are metal coordination geometry preferences imposed by the M-to- M^* barrier.

M^* formation is mediated by backbone isomerization

Our hypothesis is that divalent cation-mediated backbone isomerization of Pro32 is responsible for M^* formation. Cation binding by $\beta 2\text{m}$ occurs primarily at His31 (ref. 17). However, discrimination between Ni^{2+} and Cu^{2+} for M^* formation and subsequent oligomerization is impossible to rationalize without an additional coordinating ligand. One possibility is the amide-nitrogen lone pair at Pro32. The side chain of His31 is solvent exposed and in a position orthogonal to the Pro32 amide plane (**Fig. 4b**). The two residues should therefore be able to provide tetrahedral coordination of Cu^{2+} with minimal rearrangement. Pro32 is in a *cis* conformation and is 100% conserved¹⁷. Metal can act as a Lewis acid at Pro32, withdrawing the nitrogen lone pair and weakening the amide double bond. This has been shown to result in ~ 260 -fold acceleration of backbone isomerization in both prolyl and nonprolyl amides²⁵. Notably, the reported specificity of this catalysis is $\text{Cu}^{2+} > \text{Zn}^{2+} \gg \text{Ni}^{2+}$, which mimics our observation for $\beta 2\text{m}$ oligomerization.

To test our hypothesis, we mutated Pro32 to alanine (P32A). The frequency of nonprolyl amino acids forming *cis* bonds is $< 0.1\%$ ²⁶. Therefore, this $\beta 2\text{m}$ mutant should have a *trans* conformation at position 32 even in the absence of metal cation. Cu^{2+} binding to P32A was consistent with this prediction (**Fig. 4a**), as it bound $\sim 10,000$ -fold more tightly than WT (**Fig. 3b**). Titration of 2.5 μM P32A with Cu^{2+} resulted in a linear change in fluorescence that extrapolated to 2.6 ± 0.1 μM (**Fig. 3c**, inset). This indicated a 1:1 stoichiometry and a $K_d \ll 2.5$ μM . To quantitatively determine the K_d , Cu^{2+} binding to protein was measured in competition with glycine. This established approach has been used for other amyloid systems, including mammalian prion (PrP) from spongiform encephalopathies²⁷ and $\text{A}\beta$ peptide from Alzheimer disease²⁸. The high affinity of P32A for Cu^{2+} was apparent; for example, at 450 μM glycine and 42 μM Cu^{2+} , P32A was holo, whereas WT protein remained apo (**Fig. 3c**). The K_d of P32A for Cu^{2+} was determined to be 0.5 ± 0.1 nM (**Fig. 3b** and **Supplementary Fig. 3**

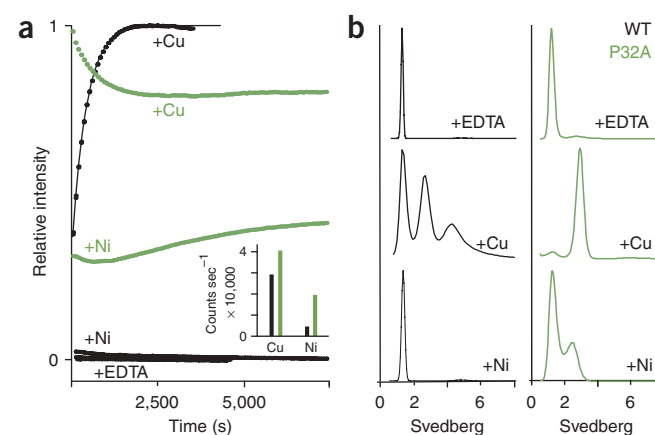


Figure 2 Discrimination between Cu^{2+} and Ni^{2+} in oligomeric assembly. **(a)** Kinetics of ThT fluorescence enhancement of WT (black) and P32A (green) at 100 μM protein upon addition of 200 μM Cu^{2+} , 300 μM Ni^{2+} or 10 mM EDTA. Kinetics for P32A and WT are separately renormalized from 0 (EDTA) to 1 (Cu^{2+}). Inset, maximum absolute intensity. **(b)** SV of 100 μM protein in the presence of 10 mM EDTA, 200 μM Cu^{2+} or 300 μM Ni^{2+} . Maximum entropy fits of $c(s)$ are shown.

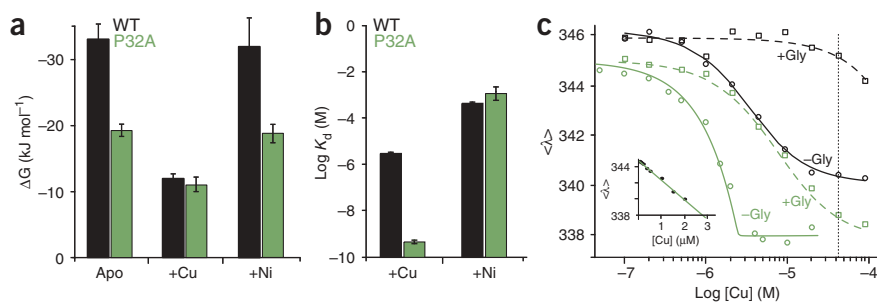


Figure 3 Differences between Cu^{2+} and Ni^{2+} in binding affinity and stability. (a) ΔG_U of 2.5 μM WT (black) or P32A (green), determined by urea denaturation¹⁷. Cation concentrations were 0 μM (apo), 90 μM Cu^{2+} and 2,000 μM Ni^{2+} . (b) Cation dissociation constants for WT (black) and P32A (green). Error bars in **a** and **b** show one s.e.m. (c) The K_d of P32A was calculated in the presence of a competing chelator, glycine. Two representative data sets are shown at 0 (solid) and 450 μM (dashed) glycine, overlaid with the global fit (all data are shown in **Supplementary Figure 3**). WT titrations under matched conditions are shown. Vertical dotted line marks 42 μM Cu^{2+} . Inset, results for 2.5 μM P32A titrated with Cu^{2+} , plotted on a linear scale. The first eight data points are shown and fit to a line.

online). Note that for WT protein, the energy difference between apo M and holo M was much less than that between apo M^* and holo M^* (**Fig. 4a**). Therefore, the increased affinity of P32A for Cu^{2+} suggests that it has adopted an M^* -like structure.

The similarities between P32A and M^* were further reflected in oligomerization and thermodynamic measurements. We have previously shown that M^* formation is the rate-limiting step governing oligomerization kinetics²³. In marked contrast to the ~ 1 -h kinetic profile of WT, Cu^{2+} -induced P32A oligomerization is complete within the measurement dead time (~ 1 min) (**Fig. 2a**). This suggests that in the native structure of P32A, the rate-limiting conversion to M^* has already taken place. This is also the likely basis of increased oligomerization efficiency for P32A (85% \pm 4% oligomer) compared to WT (67% \pm 4% oligomer) (**Fig. 2b**). The P32A mutant was folded, as judged by CD (data not shown) and NMR (**Supplementary Fig. 4** online). Notably, the Cu^{2+} -bound stability of P32A is the same as that

of WT ($\Delta\Delta G_U = 1.0$ kJ mol⁻¹; **Fig. 3a**). This suggests that little energy is required to shift the apo P32A conformation into a state that matches the M^* state of WT protein. These results reflect a strong similarity between apo P32A and the M^* state of WT protein. The importance of Cu^{2+} -catalyzed isomerization of the WT *cis*-proline was reinforced by the apparent loss of metal specificity in P32A. Oligomerization was never apparent for WT $\beta 2m$ incubated with Ni^{2+} (**Fig. 2b**). In contrast, although the affinities of P32A and WT for Ni^{2+} were comparable (**Fig. 3b**), Ni^{2+} induced an amyloid-like response in P32A (**Fig. 2a**), with 28% \pm 4% of the protein forming oligomers (**Fig. 2b**). This difference in assembly behavior was unambiguous even in controls where apo WT was chemically destabilized to match the stability of apo P32A (**Supplementary Fig. 2**). We conclude that P32A is able to adopt a conformation that Ni^{2+} -bound WT cannot. It is noteworthy that in P32A, the difference in K_d (**Fig. 3b**) between Ni^{2+} and Cu^{2+} is not reflected in the specificity of assembly. Furthermore, for P32A in the presence of Ni^{2+} , additional rearrangements occur over several hours (**Fig. 2a**). This suggests that different, albeit related, structures mediate metal-induced M^* formation and subsequent oligomer stabilization.

Molecular description of M^*

The atomic structure of P32A was solved using X-ray diffraction, providing a molecular description of M^* . The chain is complete between residues 4–97 and reveals a structure consistent with the conformation of $\beta 2m$ in complex with the MHC (PDB entry 2CLR²⁹; backbone r.m.s. deviation = 1.5 Å; **Fig. 5a**). The structure of $\beta 2m$ is a β -sandwich of four- and three-stranded sheets with connectivity ABED and CFG, respectively (**Fig. 1a**). Notably, the backbone amide between residues 31 and 32 of P32A is *trans* (**Fig. 5b**). Furthermore, His31, which is crucial to Cu^{2+} binding, adopts an alternative conformer such that it remains in a solvent-exposed position similar to that in WT.

To accommodate this *trans* peptide bond, the hydrophobic core of $\beta 2m$ is repacked. This process is likely initiated by backbone rotation of Phe30 (**Fig. 5b,c**). The benzyl side chain of Phe30 moves 8.9 Å (r.m.s. deviation) from a buried position to one with 57% solvent exposure. The benzyl group of Phe62 fills the resultant hole by moving 5.8 Å to a position only 1.6 Å (r.m.s. deviation) from Phe30 in WT $\beta 2m$ (PDB entry 2CLR). The van der Waals contact of Leu54 with Phe62 in the WT structure is lost in P32A, permitting a backbone rotation of residues 52–56. Indeed, the new position of Leu54 in P32A is 7.2 Å (r.m.s. deviation) from that in the WT structure. Additional rearrangements occur at Phe56, Tyr63 and Trp60, which move 3.7 Å, 3.5 Å and 6.3 Å, respectively. We note that NMR relaxation measurements³⁰ and ring current shifts (**Supplementary Fig. 4**) of WT $\beta 2m$ in the presence and absence of Cu^{2+} show changes consistent with perturbation of this set of residues. This probably reflects holo $\beta 2m$ transiently sampling the M^* conformation. Thus, $\beta 2m$ tolerates a *cis-trans* backbone change in its BC loop by rearranging elements that extend to the DE loop and strand D.

The structural rearrangements induced by mutation result in formation of a crystallographic dimer (**Fig. 6**). In P32A, the rotations of backbone residues 52–56 are accompanied by a 1-residue shift

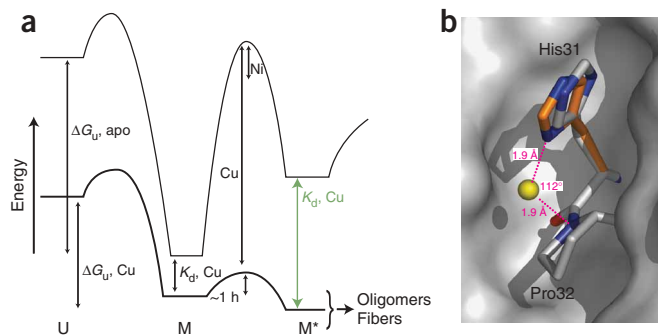


Figure 4 Energetics and Cu^{2+} -binding site of $\beta 2m$ oligomeric assembly. (a) Energy landscape for unfolded (U), native (M) and native-like (M^*) conformations of apo $\beta 2m$ (thin line) and holo $\beta 2m$ (thick line). Arrows indicate energy differences highlighted in text for WT (black) and mutant protein (green). (b) A putative Cu^{2+} -binding site of $\beta 2m$ shown in the context of the WT structure (PDB entry 2CLR).²⁹ His31 and Pro32 are shown in the context of the solvent-accessible surface. An alternative conformer of His31 has been modeled (orange), which is consistent with a tetrahedral coordination geometry for Cu^{2+} (yellow) but inconsistent with the square planar geometry preferred by Ni^{2+} .

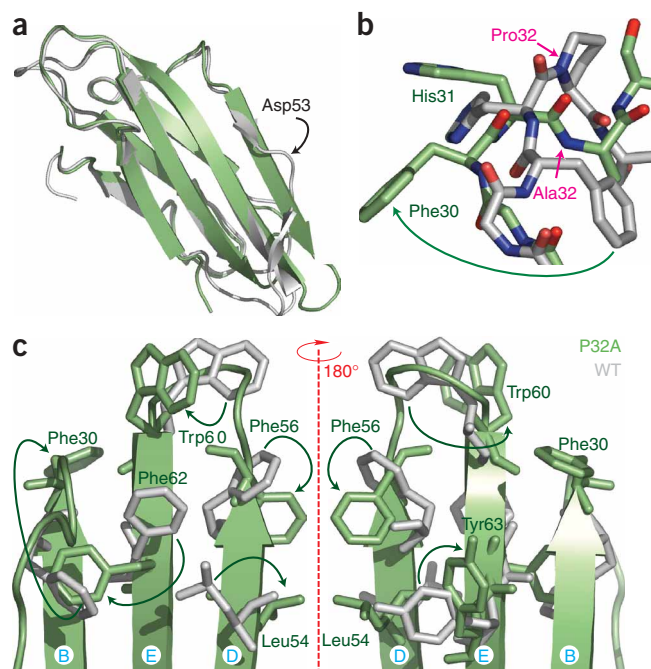


Figure 5 Structural consequences of a *trans* conformation at position 32. (a) Ribbon superposition of the P32A structure (PDB entry 2F80) and WT structure from chain B of PDB entry 2CLR²⁹. P32A is shown in green and WT in gray. Asp53 at the β -bulge in strand D of WT is indicated. (b) Residues of the BC loop. In WT, the amide at residue 32 is *cis*, whereas in P32A, it is *trans*, resulting in $\sim 180^\circ$ rotation at Phe30. (c) Summary of hydrophobic side chain differences resulting from a *trans* backbone at residue 32. Strand nomenclature from **Figure 1a** is indicated. In **b** and **c**, Phe30 is marked to indicate relative orientation.

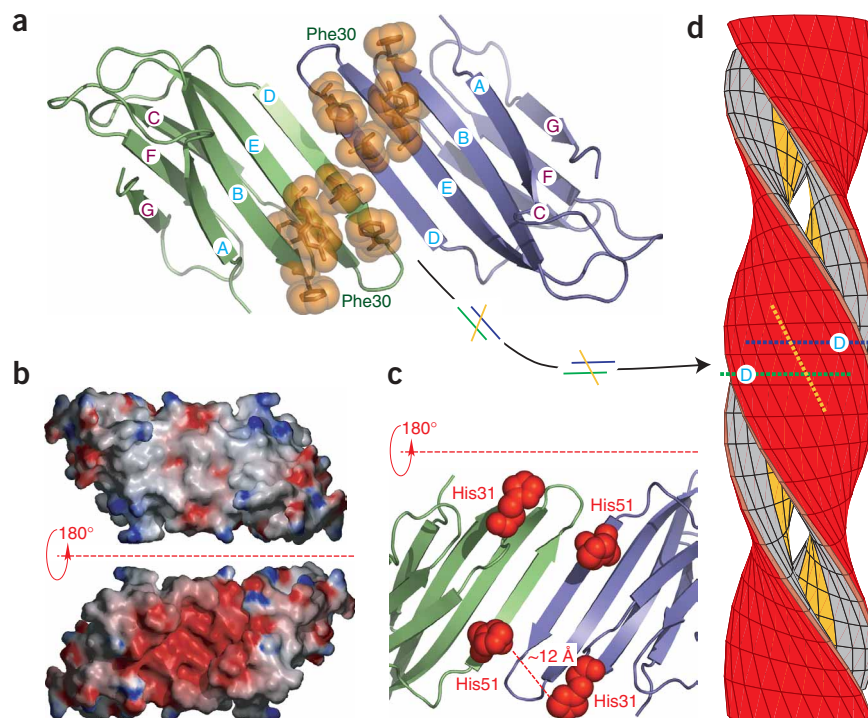
of the bulge at residue 53 (ref. 31). The crystal capture of a low-population conformer of WT β 2m (PDB entry 1LDS) also shows that the strand D β -bulge can be eliminated³². However, this results from adoption of an alternative set of intramolecular ED strand interactions. Additional disparities include a *cis* backbone for 1LDS at residue 32 and a structure 3.3 Å (r.m.s. deviation) distant from P32A. These differences appear to prevent 1LDS from adopting the dimer structure reported here. Importantly, under matched conditions, P32A crystallizes in days, whereas WT crystals are not apparent even after 4 months. These observations suggest that the structural rearrangements that accommodate a *trans* conformation at residue 32 are cooperative with the β -bulge collapse at residue 53, enabling formation of a dimerization-competent interface.

DISCUSSION

A role for metal cations has been implicated in a number of amyloid diseases. These include PrP from mammalian spongiform encephalopathies^{33,34}, A β peptide from Alzheimer disease³⁵ and α -synuclein from Parkinson disease³⁶. These systems, like β 2m, show conformational transitions that are affected by the closely related metals Cu²⁺, Zn²⁺ and Ni²⁺. For example, alternative conformations of PrP associated with different disease strains can be interconverted with Cu²⁺ (ref. 34). As with β 2m, a combination of imidazole and backbone interactions are central to these conversions³⁷. The structural

toward the C terminus. This eliminates the β -bulge at Asp53 seen in WT and results in a continuous strand D (**Fig. 5a** and **Supplementary Fig. 5** online). It has been suggested that edge-strand β -bulges serve as natural inhibitors of aggregation⁶. Indeed, the dimer of P32A is mediated by antiparallel interactions of two complete D strands (**Fig. 6a**). The units of the dimer are related by a two-fold axis normal to the plane of the D-D interaction, yielding an eight-stranded β -sheet of ABED-DEBA. In native β 2m, the observation of only limited main chain contacts (residues 54–56) can be attributed to the maintenance

Figure 6 Structural basis of amyloidogenicity. (a) Dimer of P32A viewed from above the ABED-DEBA plane. Orientation of left subunit is similar to that in **Figure 5a**. Phe30 is marked to indicate relative orientation of the subunits. A subset of the residues from **Figure 5c** (Phe30, Leu54, Phe56, Phe62 and Tyr63) are shown (orange space fills). Strand nomenclature from **Figure 1a** is indicated. (b) Solvent-accessible surface of the dimer in **a**, colored from red to blue corresponding to electrostatic potentials of -10 kT to $+10$ kT. Upper panel is in the same orientation as **a**; lower panel is rotated through 180° to show acidic face. (c) Histidine residues exposed in the acidic groove are shown as red space fills. Orientation is the same as in the lower panel of **b**. (d) An idealized single turn of two 24-stranded amphipathic β -sheets spaced 10 Å apart and coiled together with a 115-Å repeat length⁹. Interior and exterior are colored as in **b** (acidic face in red, neutral in gray). Superposed are two vertical lines corresponding to strands D-D, colored as in **a**. Here, these represent a subset of strands in the lower (occluded) sheet. Orange line corresponds to the hydrophobic stripe defined using the ζ carbon atoms of Tyr63. This closely aligns with the long axis of the upper sheet.



switch observed here and the molecular details of its propagation are, therefore, of particular value for the understanding of protein folding as well as the oligomerization of amyloids in general.

The structural changes in P32A that enable dimer formation also reveal a basis for amyloid assembly. The P32A dimer is amphipathic (Fig. 6b), a property that can support ordered in addition to amorphous aggregation. Notably, the hydrophobic face is populated by residues with positions altered relative to WT. These residues create a stripe at $\sim 65^\circ$ across strands ABED-DEBA (Fig. 6a). A twisted pair of extended sheets formed from these dimers will therefore maintain burial of this hydrophobic stripe at a sheet-to-sheet crossing angle of $\sim 130^\circ$. This is consistent with canonical dimensions⁹ for amyloid fibers and leads to the prediction that the cross- β core is formed from only the ABED strands (Fig. 6d). These strands would have an arrangement alternating head-to-head (that is, D-D) and tail-to-tail (that is, A-A); a similar arrangement has recently been suggested for the assembly of the NM domain from the yeast prion³⁸. A noteworthy feature of our model is its assembly from native-like precursors, as a partially folded or unfolded state of $\beta 2m$ is unlikely to provide the discrimination we observed between Ni^{2+} and Cu^{2+} . This is supported by our observation that stoichiometric Cu^{2+} gives rise to amyloid formation but is not destabilizing²³. In addition, spectroscopic evidence enabled us to suggest that $\beta 2m$ assembles from native-like precursors. Once formed, however, $\beta 2m$ fibers are resistant to the addition of chelate¹⁵. Therefore, given the close proximity of native-like states in our model, a three-dimensional domain-swapped mechanism^{39,40}, such as that observed in cystatin⁴¹ or RNase⁴², may provide for the subsequent changes in mature amyloid. Our structure of P32A (M^*), although greatly perturbed at particular residues, is native-like and represents an intermediate on this pathway.

The hydrophobic face of the P32A dimer is opposed by an acidic groove bracketed by the CFG sheets (Fig. 6b). Therefore, charge repulsion is probably the cause of the little apparent apo P32A oligomerization in dilute solution. After M^* formation, divalent cations are required for the oligomerization of WT protein²³ and P32A. The reason for this is likely to be charge neutralization of the acidic groove. Likely participants in such an event are His31 and His51, which reside in this groove, $\sim 12 \text{ \AA}$ apart (Fig. 6c). These observations may also explain the ability of $\beta 2m$ to form fibers at low pH (< 5)⁴³ without addition of Cu^{2+} . Acidic and divalent-cation pathways are consistent if protonation mimics the charge effects of Cu^{2+} binding and if Pro32 in acid-destabilized $\beta 2m$ samples the *trans* conformation. Indeed, a slow refolding step of acid-unfolded $\beta 2m$ has been attributed to the presence of a *trans* conformation at Pro32 (ref. 44).

In summary, Cu^{2+} catalyzes formation of an activated state, tethers two molecules of $\beta 2m$ together to form an amphipathic eight-stranded sheet and reduces charge repulsion to facilitate association of dimers in a process that precedes and correlates with the formation of amyloid. The structural basis of this is the capacity of native $\beta 2m$ to accommodate both *cis* and *trans* isomers of its backbone at a buried ($\sim 15\%$ solvent exposed) and conserved site. In apo $\beta 2m$, the *cis* conformer is more stable; however, the *trans* conformer is specifically accessed and then stabilized by interactions with Cu^{2+} . Backbone isomerization of both prolyl⁴⁵ and nonprolyl⁴⁶ peptide bonds is typically associated with slow refolding. It is also implicated in conformational changes associated with functional regulation⁴⁷, such as the opening of an ion channel⁴⁸. As slow refolding and conformational changes are both factors in aggregation, catalysis of these phenomena is the likely origin of the increasingly observed importance of metal cations in amyloid formation.

Table 1 Data collection and refinement statistics

	P32A
Data collection	
Space group	$P4_32_12$
Cell dimensions	
a, b, c (Å)	89.95, 89.95, 54.76
α, β, γ (°)	90.00, 90.00, 90.00
Resolution (Å)	50.0–1.7 (1.76–1.70) ^a
R_{sym} or R_{merge}	0.059 (0.827)
$I / \sigma I$	27.0 (2.0)
Completeness (%)	99.8 (99.6)
Redundancy	6.0 (5.3)
Refinement	
Resolution (Å)	50.0–1.70
No. reflections	25,232
R_{work} / R_{free}	18.4 / 22.7
No. atoms	1,915
Protein	1,564
Ligand/ion	
Water	351
B-factors	
Protein	37.87
Ligand/ion	
Water	59.06
R.m.s. deviations	
Bond lengths (Å)	0.008
Bond angles (°)	1.091

^aHighest-resolution shell is shown in parentheses. One crystal was used to solve this structure.

METHODS

Materials. WT protein was obtained from the urine of Dent disease patients and from *E. coli* expression as previously described²³. In both cases, purity of $> 95\%$ was determined by SDS-PAGE and electro-spray ionization MS. The oxidation state of the disulfide bond between Cys25 and Cys80 was verified as previously described¹⁷. The P32A mutation was made using the QuikChange kit (Stratagene) and confirmed by sequencing (Keck facility, Yale University).

Stability and binding. Stability and metal-binding of $\beta 2m$ were measured by changes in average emission wavelength, $\langle \lambda \rangle$, as previously described¹⁷. K_d of Cu^{2+} for P32A was determined from separate titrations in the presence of 0–900 μM glycine. A simultaneous fit of all the data to a system of mass-action equilibria was performed. K_d of Cu^{2+} for $\beta 2m$ was the only floating parameter. The pH-corrected K_d s of glycine for Cu^{2+} were from published values⁴⁹. Baselines were set at 338.0 for holo $\beta 2m$ and 345.0 for apo $\beta 2m$. ΔG_U measurements⁵⁰ were made as previously described¹⁷ and allowed to equilibrate for at least 6 h. Calculations and modeling of Figure 6d were done using Mathematica 5.1 (Wolfram Research Inc.). All errors given are \pm s.e.m.

Oligomerization. Oligomers of $\beta 2m$ were formed and detected by SV as previously described²³. SV data analysis assumed a spherical shape and used the continuous $c(s)$ distribution model, independent species model and confidence interval in M features of Sedfit v8.5 (ref. 51). All SV curves were renormalized to an equal height for the largest peak of each scan. Kinetic measurements were made using ThT as previously described²³. Measurement dead time was ~ 1 min, and ThT fluorescence enhancement was monitored at 440 and 492 nm for emission scans. Corrected lamp intensity was used.

Crystallization. P32A crystals were grown in 3- μl hanging drops with 31% (w/v) PEG 4000, 25% (v/v) glycerol, 0.2 M ammonium acetate and 0.1 M sodium acetate (pH 5.6). Drops consisted of 1 μl ~ 19 mg ml^{-1} protein, 1 μl mother liquor and 1 μl 0.05 M sodium acetate (pH 5.6). Crystals were frozen directly from the drop with liquid nitrogen. Crystals with dimensions of $0.2 \times 0.2 \times 0.1$ mm formed within 16 d at 22 °C.

Structure determination and refinement. X-ray data were collected at beamline X25 at the National Synchrotron Light Source. Data were integrated and scaled using the HKL2000 program suite⁵². A molecular-replacement solution was determined using Phaser⁵³ by searching for two copies of a truncated model of the structure in PDB entry 1LDS (residues 0–11, 21–44, 62–70 and 75–96). Model bias was reduced using the prime and switch feature of RESOLVE⁵⁴, and the chains were completed using ARP/wARP⁵⁵. Iterative cycles of building and refinement using O⁵⁶, REFMAC5 (ref. 57) and CNS⁵⁸ led to a working R_{work} of 18.4% and an R_{free} of 22.7%. Molecular graphics were prepared using PyMOL (<http://pymol.sourceforge.net>). Electrostatic potentials were calculated in GRASP⁵⁹ and rendered using POV-Ray (<http://www.povray.org>). R.m.s. deviations were calculated in lsqkab⁵⁷. Two chains reside in the asymmetric unit, related by a noncrystallographic two-fold axis. The r.m.s. deviation between all atoms of the two chains is 1.5 Å, and all residues have proper geometry; no residues fall within the disallowed regions of the Ramachandran diagram. All discussion in this paper pertains to chain A (Table 1).

Accession codes. Protein Data Bank: Coordinates have been deposited with accession code 2F8O.

Note: Supplementary information is available on the Nature Structural & Molecular Biology website.

ACKNOWLEDGMENTS

We thank L. J. Regan and T. A. Steitz for careful reading of this work and D. E. Engelman and S. A. Strobel for the use of their instruments. We also thank D. Blaho, M. Calabrese, J. Cochrane, S. Kamtekar, M. Strickler, A. Valentine and the staff of the Center for Structural Biology and National Synchrotron Light Source beamline X25 for assistance and helpful discussions. This work was supported by the US National Institutes of Health (grants DK54899 and 1F31NS046937).

COMPETING INTERESTS STATEMENT

The authors declare that they have no competing financial interests.

Published online at <http://www.nature.com/nsmb/>

Reprints and permissions information is available online at <http://npg.nature.com/reprintsandpermissions/>

- Dobson, C.M. Protein folding and misfolding. *Nature* **426**, 884–890 (2003).
- Selkoe, D.J. Folding proteins in fatal ways. *Nature* **426**, 900–904 (2003).
- Chapman, M.R. *et al.* Role of *Escherichia coli* curli operons in directing amyloid fiber formation. *Science* **295**, 851–855 (2002).
- Huff, M.E., Balch, W.E. & Kelly, J.W. Pathological and functional amyloid formation orchestrated by the secretory pathway. *Curr. Opin. Struct. Biol.* **13**, 674–682 (2003).
- Si, K., Lindquist, S. & Kandel, E.R. A neuronal isoform of the alypsia CPEB has prion-like properties. *Cell* **115**, 879–891 (2003).
- Richardson, J.S. & Richardson, D.C. Natural beta-sheet proteins use negative design to avoid edge-to-edge aggregation. *Proc. Natl Acad. Sci. USA* **99**, 2754–2759 (2002).
- Stefani, M. & Dobson, C.M. Protein aggregation and aggregate toxicity: new insights into protein folding, misfolding diseases and biological evolution. *J. Mol. Med.* **81**, 678–699 (2003).
- Caughey, B. & Lansbury, P.T., Jr. Protofibrils, pores, fibrils, and neurodegeneration: separating the responsible protein aggregates from the innocent bystanders. *Annu. Rev. Neurosci.* **26**, 267–298 (2003).
- Sunde, M. *et al.* Common core structure of amyloid fibrils by synchrotron X-ray diffraction. *J. Mol. Biol.* **273**, 729–739 (1997).
- Bjorkman, P.J. *et al.* Structure of the human class-I histocompatibility antigen, Hla-A2. *Nature* **329**, 506–512 (1987).
- Solheim, J.C. Class I MHC molecules: assembly and antigen presentation. *Immunol. Rev.* **172**, 11–19 (1999).
- Drueke, T.B. Beta2-microglobulin and amyloidosis. *Nephrol. Dial. Transplant.* **15** Suppl 1, 17–24 (2000).
- Malaguarnera, M. *et al.* Serum beta2-microglobulin in chronic hepatitis C. *Dig. Dis. Sci.* **42**, 762–766 (1997).
- Keating, M.J. Chronic lymphocytic leukemia. *Semin. Oncol.* **26**, 107–114 (1999).
- Eakin, C.M. & Miranker, A.D. From chance to frequent encounters: origins of beta2-microglobulin fibrillogenesis. *Biochim. Biophys. Acta* **1753**, 92–99 (2005).
- Okon, M., Bray, P. & Vucelic, D. ¹H NMR assignments and secondary structure of human β 2-microglobulin in solution. *Biochemistry* **31**, 8906–8915 (1992).
- Eakin, C.M., Knight, J.D., Morgan, C.J., Gelfand, M.A. & Miranker, A.D. Formation of a copper specific binding site in non-native states of beta-2-microglobulin. *Biochemistry* **41**, 10646–10656 (2002).
- McParland, V.J. *et al.* Partially unfolded states of beta(2)-microglobulin and amyloid formation in vitro. *Biochemistry* **39**, 8735–8746 (2000).
- Jones, S., Manning, J., Kad, N.M. & Radford, S.E. Amyloid forming peptides from beta(2)-microglobulin-insights into the mechanism of fibril formation in vitro. *J. Mol. Biol.* **325**, 249–257 (2003).
- Esposito, G. *et al.* Removal of the N-terminal hexapeptide from human beta2-microglobulin facilitates protein aggregation and fibril formation. *Protein Sci.* **9**, 831–845 (2000).
- Morgan, C.J., Gelfand, M., Atreya, C. & Miranker, A.D. Kidney dialysis-associated amyloidosis: a molecular role for copper in fiber formation. *J. Mol. Biol.* **309**, 339–345 (2001).
- Vorbeck-Meister, I., Sommer, R., Vorbeck, F. & Horl, W.H. Quality of water used for haemodialysis: bacteriological and chemical parameters. *Nephrol. Dial. Transplant.* **14**, 666–675 (1999).
- Eakin, C.M., Attenello, F.J., Morgan, C.J. & Miranker, A.D. Oligomeric assembly of native-like precursors precedes amyloid formation by beta-2 microglobulin. *Biochemistry* **43**, 7808–7815 (2004).
- LeVine, H., III. Thioflavine T interaction with synthetic Alzheimer's disease beta-amyloid peptides: detection of amyloid aggregation in solution. *Protein Sci.* **2**, 404–410 (1993).
- Cox, C. & Lectka, T. Synthetic catalysis of amide isomerization. *Acc. Chem. Res.* **33**, 849–858 (2000).
- Jabs, A., Weiss, M.S. & Hilgenfeld, R. Non-proline cis peptide binds in proteins. *J. Mol. Biol.* **286**, 291–304 (1999).
- Jones, C.E., Abdelraheim, S.R., Brown, D.R. & Viles, J.H. Preferential Cu²⁺ coordination by His96 and His111 induces beta-sheet formation in the unstructured amyloidogenic region of the prion protein. *J. Biol. Chem.* **279**, 32018–32027 (2004).
- Atwood, C.S. *et al.* Characterization of copper interactions with alzheimer amyloid beta peptides: identification of an attomolar-affinity copper binding site on amyloid beta1–42. *J. Neurochem.* **75**, 1219–1233 (2000).
- Collins, E.J., Garboczi, D.N. & Wiley, D.C. Three-dimensional structure of a peptide extending from one end of a class I MHC binding site. *Nature* **371**, 626–629 (1994).
- Villanueva, J. *et al.* Increase in the conformational flexibility of beta 2-microglobulin upon copper binding: a possible role for copper in dialysis-related amyloidosis. *Protein Sci.* **13**, 797–809 (2004).
- Rosano, C. *et al.* beta2-microglobulin H31Y variant 3D structure highlights the protein natural propensity towards intermolecular aggregation. *J. Mol. Biol.* **335**, 1051–1064 (2004).
- Trinh, C.H., Smith, D.P., Kalverda, A.P., Phillips, S.E. & Radford, S.E. Crystal structure of monomeric human beta-2-microglobulin reveals clues to its amyloidogenic properties. *Proc. Natl Acad. Sci. USA* **99**, 9771–9776 (2002).
- Stockel, J., Safar, J., Wallace, A.C., Cohen, F.E. & Prusiner, S.B. Prion protein selectively binds copper(II) ions. *Biochemistry* **37**, 7185–7193 (1998).
- Wadsworth, J.D. *et al.* Strain-specific prion-protein conformation determined by metal ions. *Nat. Cell Biol.* **1**, 55–59 (1999).
- Bush, A.I. The metallobiology of Alzheimer's disease. *Trends Neurosci.* **26**, 207–214 (2003).
- Rasia, R. *et al.* Structural characterization of copper(II) binding to alpha-synuclein: insights into the bioinorganic chemistry of Parkinson's disease. *Proc. Natl Acad. Sci. USA* **102**, 4294–4299 (2005).
- Jones, C., Kiewpatinond, M., Abdelraheim, S., Brown, D. & Viles, J. Probing copper²⁺ binding to the prion protein using diamagnetic nickel²⁺ and ¹H NMR: the unstructured N terminus facilitates the coordination of six copper²⁺ ions at physiological concentrations. *J. Mol. Biol.* **346**, 1393–1407 (2005).
- Krishnan, R. & Lindquist, S.L. Structural insights into a yeast prion illuminate nucleation and strain diversity. *Nature* **435**, 765–772 (2005).
- Miranker, A.D. Structural biology: fibres hinge on swapped domains. *Nature* **437**, 197–198 (2005).
- Liu, Y. & Eisenberg, D. 3D domain swapping: as domains continue to swap. *Protein Sci.* **11**, 1285–1299 (2002).
- Sanders, A. *et al.* Cystatin forms a tetramer through structural rearrangement of domain-swapped dimers prior to amyloidogenesis. *J. Mol. Biol.* **336**, 165–178 (2004).
- Sambashivan, S., Liu, Y., Sawaya, M.R., Gingery, M. & Eisenberg, D. Amyloid-like fibrils of ribonuclease A with three dimensional domain-swapped and native-like structure. *Nature* **437**, 266–269 (2005).
- Radford, S.E., Gosal, W.S. & Platt, G.W. Towards an understanding of the structural molecular mechanism of beta(2)-microglobulin amyloid formation in vitro. *Biochim. Biophys. Acta* **1753**, 51–63 (2005).
- Kameda, A. *et al.* Nuclear magnetic resonance characterization of the refolding intermediate of beta2-microglobulin trapped by non-native prolyl peptide bond. *J. Mol. Biol.* **348**, 383–397 (2005).
- Wedemeyer, W.J., Welker, E. & Scheraga, H.A. Proline *cis-trans* isomerization and protein folding. *Biochemistry* **41**, 14637–14644 (2002).
- Pappenberger, G. *et al.* Nonprolyl *cis* peptide bonds in unfolded proteins cause complex folding kinetics. *Nat. Struct. Biol.* **8**, 452–458 (2001).
- Andreotti, A.H. Native state proline isomerization: an intrinsic molecular switch. *Biochemistry* **42**, 9515–9524 (2003).
- Lumms, S.C. *et al.* *Cis-trans* isomerization at a proline opens the pore of a neurotransmitter-gated ion channel. *Nature* **438**, 248–252 (2005).

49. Dawson, R.M., Elliot, D.C., Elliot, W.H. & Jones, K.M. *Data for Biochemical Research* 3rd edn (Clarendon Press, Oxford, 1986).
50. Bolen, D.W. & Santoro, M.M. Unfolding free energy changes determined by the linear extrapolation method. 2. Incorporation of delta G degrees N-U values in a thermodynamic cycle. *Biochemistry* **27**, 8069–8074 (1988).
51. Schuck, P. Size-distribution analysis of macromolecules by sedimentation velocity ultracentrifugation and lamm equation modeling. *Biophys. J.* **78**, 1606–1619 (2000).
52. Otwinowski, Z. & Minor, W. Processing of X-ray diffraction data collected in oscillation mode. *Methods Enzymol.* **276**, 307–326 (1997).
53. Storoni, L.C., McCoy, A.J. & Read, R.J. Likelihood-enhanced fast rotation functions. *Acta Crystallogr. D Biol. Crystallogr.* **60**, 432–438 (2004).
54. Terwilliger, T.C. Maximum-likelihood density modification. *Acta Crystallogr. D Biol. Crystallogr.* **56**, 965–972 (2000).
55. Perrakis, A., Morris, R. & Lamzin, V.S. Automated protein model building combined with iterative structure refinement. *Nat. Struct. Biol.* **6**, 458–463 (1999).
56. Jones, T.A., Zou, J.Y., Cowan, S.W. & Kjeldgaard, M. Improved methods for building protein models in electron density maps and the location of errors in these models. *Acta Crystallogr. A* **47**, 110–119 (1991).
57. Collaborative Computational Project, Number 4. The CCP4 suite: programs for protein crystallography. *Acta Crystallogr. D Biol. Crystallogr.* **50**, 760–763 (1994).
58. Brunger, A.T. *et al.* Crystallography & NMR system: A new software suite for macromolecular structure determination. *Acta Crystallogr. D Biol. Crystallogr.* **54**, 905–921 (1998).
59. Nicholls, A., Sharp, K.A. & Honig, B. Protein folding and association: insights from the interfacial and thermodynamic properties of hydrocarbons. *Proteins* **11**, 281–296 (1991).